



# nature 1 photonics

OCTOBER 2009 VOL 3 NO 10  
[www.nature.com/naturephotonics](http://www.nature.com/naturephotonics)

**EXCITONICS**  
Switches warm up

**ULTRAVIOLET SOURCES**  
Boron nitride alternative

**WAVEFORM GENERATION**  
Ultrafast answer

**Liquid-crystal microresonators**

# Electrically tunable liquid crystal optical microresonators

M. Humar<sup>1</sup>, M. Ravnik<sup>2</sup>, S. Pajk<sup>3</sup> and I. Muševič<sup>1,2,\*</sup>

**Because of their small mode volume and high Q-factors, optical microresonators are interesting for applications such as laser sources, active filters and all-optical switches. Especially interesting are tunable resonators, in which the resonance frequency tuning by size, shape, temperature or electric field can be achieved. Here we demonstrate electrically tunable, low-loss whispering-gallery-mode (WGM) resonators made of nematic liquid crystal droplets, embedded in a polymer matrix. The shift in resonant frequencies is achieved via electric field-induced structural distortion of the birefringent liquid crystal resonator medium. Nematic liquid crystal microresonators have a large tuning range of the order of 20 nm at  $2.6 \text{ V } \mu\text{m}^{-1}$  for a  $\sim 600 \text{ nm}$  WGM in  $17\text{-}\mu\text{m}$ -diameter droplets and high Q-factors up to  $\sim 12,000$  in  $33\text{-}\mu\text{m}$ -diameter droplets. The tunability is approximately two orders of magnitude larger than usually achieved in solid-state microresonators.**

In spherical microresonators<sup>1</sup> the light is trapped inside a microsphere by total internal reflection at the interface between the microsphere and the surrounding medium. The light can be considered circulating inside the microsphere by multiple total internal reflections at the interface. The resonance condition for circulating light is fulfilled if the light reaches the original point with the same phase after one circulation. These kind of resonances are usually referred to as whispering-gallery-modes (WGMs) or morphology-dependent resonances. They usually have small mode volumes and very high Q-factors and are therefore interesting for applications such as laser sources, active filters and all-optical switches<sup>2</sup>. Especially interesting are tunable resonators, in which resonance frequency tuning by size, shape, temperature or electric field has been reported. Mechanical shape control results in large frequency shifts<sup>3,4</sup>, but is slow, inaccurate and impractical for real applications. Electrical tuning of solid-state microresonators simplifies integration with other electric components, but the shift of the resonant frequencies is usually quite small<sup>5–8</sup>.

Nematic liquid crystals (NLCs) are orientationally ordered, optically uniaxial complex fluids, in which rod-like molecules are preferentially aligned into a direction dictated by the external field or confining surfaces<sup>9</sup>. When an external a.c. electric field is applied to a NLC sandwiched between confining surfaces, molecules tend to align with their long axes into the field direction to minimize the elastic and electric energy. This causes collective reorientations of NLC molecules, and the liquid crystal is elastically distorted. As the NLC molecules are usually strongly anchored at the confining surfaces of the device, the elastic deformation provides restoring torques, which drive the NLC into an original configuration, once the field is switched off. Owing to their high birefringence (typically 0.1–0.2) and large optical response to the external electric field, NLCs are now widely used in liquid-crystal displays, two-dimensional spatial light modulators and optical switches. Electrically tunable optical devices such as cholesteric liquid-crystal lasers<sup>10–15</sup>, beam-steering devices with a liquid-crystal cladding layer, tunable two-dimensional photonic nematic colloidal crystals<sup>16</sup> and solid-state optical microresonators with a NLC cladding layer<sup>5</sup> have been demonstrated.

Here we show that small nematic droplets embedded in a polymer matrix are low-loss optical microresonators, which can be tuned efficiently by an external electric field. The orientation of liquid-crystal (LC) molecules at the surface of the microresonators is perpendicular, resulting in a radial nematic structure with a topological defect in the centre. The optical tunability is achieved by electric-field-induced elastic structural deformation of the nematic LC, filling the cavity. This changes the index of refraction for light circulating inside the birefringent microcavity and induces a WGM shift with increasing electric field.

## Nematic liquid crystal droplet microresonators

Liquid-crystal microresonators are spherical LC microdroplets, suspended in a supporting polymer matrix. They were prepared by mixing a small amount ( $\sim 5\%$ ) of fluorescently labelled NLC E12 (a commercial mixture of cyanobiphenyl NLCs) and polydimethylsiloxane (PDMS). Polymer dispersions of NLC droplets have been studied extensively in the past<sup>17</sup>, but individual droplets have never been considered as tunable optical resonators.

A micrograph of a typical microdroplet of E12 in PDMS is shown in unpolarized light and between crossed polarizers in Fig. 1a,b, respectively. A uniaxial cross in Fig. 1b clearly indicates that the internal structure of the director field, describing molecular orientation inside a spherical cavity, is radial<sup>18</sup>, as shown schematically in Fig. 1c. This means that NLC molecules are aligned perpendicularly to the surface of the microcavity, which creates splay elastic distortion of the NLC<sup>9</sup>; and a point topological defect, called the radial hedgehog defect appears in the centre of the droplet<sup>19</sup>. We observe fluorescence only inside the NLC droplets, which indicates that the dye has not diffused into the surrounding PDMS.

When the dye-doped E12 microdroplet of  $\sim 10 \mu\text{m}$  diameter was illuminated with a tightly focused 514 nm laser beam near its edge, a bright spot was observed on the other side of the droplet as can be seen in Fig. 1d. A stripe of light in between these two points, which is in fact a light ring along the circumference of the microcavity, is also clearly visible, which means that we are observing WGMs in a LC droplet. The analysis of the polarization shows that the WGM mode is polarized along the line that connects the two bright

<sup>1</sup>J. Stefan Institute, Jamova 39, SI-1000, Ljubljana, Slovenia, <sup>2</sup>Faculty of Mathematics and Physics, University of Ljubljana, Jadranska 19, SI-1000, Ljubljana, Slovenia, <sup>3</sup>Faculty of Pharmacy, University of Ljubljana, Aškerčeva 7, SI-1000, Ljubljana, Slovenia. \*e-mail: igor.musevic@ijs.si

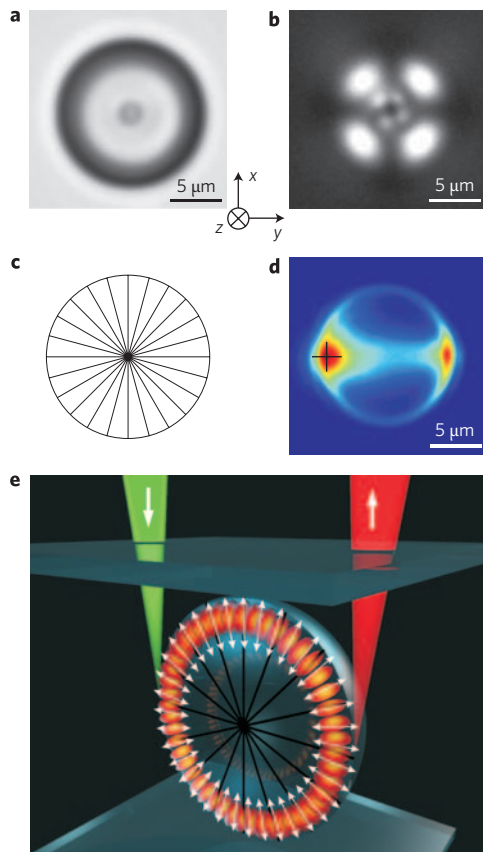


**Figure 1 | Light in liquid-crystal microdroplets.** **a**, Microdroplet of nematic liquid crystal E12 in PDMS. **b**, The same droplet under crossed polarizers. **c**, Structure of the director field inside the microdroplet, deduced from **b**. The lines (that is, the director field) present the direction of orientation of LC molecules. **d**, Detected light intensity under illumination by a strongly focused beam of the Ar<sup>+</sup> laser tweezers, illuminating the submicrometre-sized spot near the rim of the droplet, indicated by the black cross. **e**, Schematic view of the excitation of WGMs in a LC droplet by a focused Ar<sup>+</sup> laser (green light illuminating the spot on the droplet), and detection of the radiated WGM light (red light). A TM WGM is shown, with its electric field oscillating in a radial direction.

spots. The intensity profile and the polarization indicate that the light circulates mainly in the  $y$ - $z$  plane and that the electric field of the WGM is oscillating in the radial direction, as illustrated in Fig. 1e and in more detail in Supplementary Figs S1 and S2. The WGM is therefore a transverse magnetic (TM) mode, which is in agreement with the structure of the NLC inside the microresonator. Namely, as the LC molecules are oriented perpendicularly to the surface of the microresonator (shown by black radial lines in Fig. 1e), the two transverse electric (TE) and TM polarizations sense quite different refractive indices during their circulation. The TM polarization, with its electric field oscillating in a radial direction, (see Supplementary Fig. S2) senses a larger dielectric constant along the long axis of the molecules, corresponding to the extraordinary index ( $n_e = 1.74$ ). On the other hand, the electric field of the TE mode oscillates perpendicularly to the long axis of the molecules (Supplementary Fig. S2) and senses the ordinary index, which is much lower ( $n_o = 1.52$ ). Taking into account the refractive index of the surrounding PDMS ( $n_s = 1.43$ ), only TM modes have an index contrast large enough to be supported by a small NLC microresonator.

The spectrum of light, emitted from a 10- $\mu\text{m}$ -diameter E12 microdroplet in PDMS is presented in Fig. 2a. WGM resonances are clearly resolved above the fluorescent background. We observe

that for this size droplet, only one polarization is supported by the resonator and this set of modes corresponds to the fundamental ( $n = 1$ ) WGM TM modes<sup>20</sup>. Here,  $n$  is the radial number of the mode, which determines the number of maxima in the radial intensity distribution inside the sphere<sup>20</sup>. A single set of fundamental modes is a quite unique feature of NLC microresonators compared with other similar systems, which usually have both polarizations present. However, the WGM spectrum from a larger (12.6  $\mu\text{m}$ ) droplet of E12, seen in Fig. 2b, shows an additional set of WGM resonances, which correspond to higher radial TM modes. In even larger droplets, we expect that the TE modes would appear as well. Mode numbers in Fig. 2a,b were determined by fitting the experimental spectra to the resonant frequencies, as calculated within the theory of WGMs in radial anisotropic dielectric microspheres. As the material parameters are not known exactly, the angular mode numbers  $l$  are determined with the precision of  $\pm 1$ .

The inset to Fig. 2b shows details in a narrow band of the WGM spectra, measured with a high-resolution micro-Raman spectrometer in a 53- $\mu\text{m}$ -diameter droplet. The linewidth of the resonance is very low,  $\Delta\lambda = 0.055$  nm, and the LC cavity  $Q$ -factor is of the order of  $\sim 12,000$ . This means that losses due to scattering of light on thermally induced orientational fluctuations of LC molecules are very small<sup>9</sup>. The  $Q$ -factor depends on the size of the droplet and losses due to leakage, but is still very high: we obtain  $Q \approx 4,000$ – $6,000$  in 10–13  $\mu\text{m}$  droplets and  $Q > 10,000$  in droplets larger than 30  $\mu\text{m}$ . Linewidths of emission lines that have been reported in lasing experiments in liquid crystals are of the order of 0.3–0.4 nm in dye-doped cholesteric liquid crystals<sup>12,13</sup>, 0.11 nm in dye-doped liquid crystal blue phases<sup>14</sup>, and 0.06 nm in order-parameter optimized dye-doped cholesteric liquid crystals<sup>15</sup>.

### Theory of WGMs in anisotropic microspheres

In general, WGMs are decomposed components of the full electric field in the resonator and therefore have to satisfy Maxwell's equations for the given dielectric profile and surface conditions. To characterize the observed spectra in our spherical birefringent microresonators, where the local optical axis points into the radial direction, we calculated the resonant frequencies by using analytical solutions of Mie type for the electric and magnetic field, as obtained in ref. 21. The electric field in a given mode is uniquely characterized by the polarization (TE or TM) and three mode numbers  $n$ ,  $l$  and  $m$ , corresponding to the radial, azimuthal and polar directions, respectively. The electric field  $\mathbf{E}$  and magnetic field  $\mathbf{H}$  are expanded into a series of eigenfunctions. In spherical geometry, with spherically symmetric dielectric permittivity and magnetic permeability, the eigenfunctions in radial direction are spherical Bessel or spherical Hankel functions of the first kind, whereas in the azimuthal and polar directions the eigen-functions are spherical harmonics<sup>21</sup>. Here we show only the constitutive equations for the radial functions  $Z_l^{(a)}(kr)$  and  $Z_l^{(b)}(kr)$ , which determine the radial profile of both electric and magnetic field:

$$\frac{1}{r} \left( \frac{\partial}{\partial r} \right)^2 \left( r Z_l^{(a)}(kr) \right) + \left[ k^2 - \frac{l(l+1) \mu_o}{r^2} \right] Z_l^{(a)}(kr) = 0 \quad (1)$$

$$\frac{1}{r} \left( \frac{\partial}{\partial r} \right)^2 \left( r Z_l^{(b)}(kr) \right) + \left[ k^2 - \frac{l(l+1) i \omega \epsilon_o + \sigma_o}{r^2} \right] Z_l^{(b)}(kr) = 0 \quad (2)$$

Here,  $\mu_o$  ( $\mu_e$ ) is the ordinary (extraordinary) magnetic permeability,  $\epsilon_o$  ( $\epsilon_e$ ) is the ordinary (extraordinary) dielectric permittivity,  $\sigma_o$  ( $\sigma_e$ ) is the ordinary (extraordinary) electric conductivity, and the complex wave vector  $k^2 = \mu_o \epsilon_o \omega^2 / c^2 - i \mu_o \sigma_o \omega$ .  $c$  is the speed of light in a vacuum and  $\mu_o$  is the induction constant. Liquid-crystal

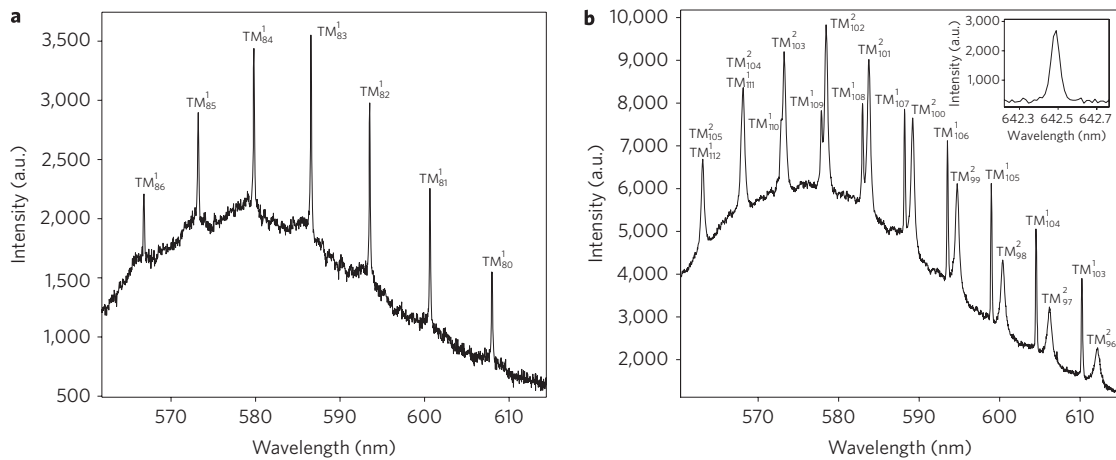


**Figure 2 | Spectrum of light circulating in a liquid-crystal droplet.** **a**, A single set of WGM resonances is observed in a 10.1 μm droplet of E12 in PDMS, corresponding to the lowest radial modes ( $n = 1$ ) with TM polarization. **b**, In a larger radial birefringent droplet (12.6 μm) second radial modes appear with  $n = 2$ . The inset shows details of a WGM spectral line in a 53 μm-diameter E12 droplet. The linewidth is approximately 0.055 nm, and the LC cavity Q-factor is of the order of  $\sim 12,000$ . This spectrum was measured using a high-resolution micro-Raman spectrophotometer.

materials have their ordinary and extraordinary permeabilities close to unity,  $\mu_o, \mu_e \sim 1 + 10^{-6}$  (ref. 9), therefore one can approximate  $\mu_o/\mu_e \approx 1$ . In addition, they are typically not conductive, so it can be assumed that  $\sigma_o = \sigma_e = 0$ . Note, that the assumption that  $\mu_o = \mu_e = 1$  implies that  $n_o = \sqrt{\epsilon_o}$  and  $n_e = \sqrt{\epsilon_e}$ . These approximations simplify equations 1 and 2, such that  $Z_l^{(a)}(kr)$  is identified as a spherical Bessel or spherical Hankel function  $Z_l^{(a)}(kr) = \{j_l\}_l(kr)$ , respectively, with integer order  $l$ , whereas  $Z_l^{(b)}(kr)$  is a spherical Bessel or spherical Hankel function  $Z_l^{(b)}(kr) = \{j_l\}_l(kr)$  with non-integer order  $\tilde{l} = \tilde{l}(l) = (-1 + \sqrt{1 + 4(n_o/n_e)^2 l(l+1)})/2$ . Having determined the radial functions, one can write the full electric field and magnetic field inside (spherical Bessel functions) and outside (spherical Hankel functions) the resonator. After coupling the solutions for either TE or TM polarization at the surface of the resonator, characteristic equations are obtained for the resonant frequencies  $\omega_{nl}$  in dielectrically anisotropic sphere, with local optical axis in the radial direction (radial anisotropic sphere):

$$-j_l(\phi_{nl}) \left[ h_l(\tilde{\phi}_{nl}) + \tilde{\phi}_{nl} \frac{\partial h_l(x)}{\partial x} \Big|_{\tilde{\phi}_{nl}} \right] + h_l(\tilde{\phi}_{nl}) \left[ j_l(\phi_{nl}) + \phi_{nl} \frac{\partial j_l(x)}{\partial x} \Big|_{\phi_{nl}} \right] = 0 \tag{3}$$

$$-j_{\tilde{l}}(\phi_{nl}) \left[ h_{\tilde{l}}(\tilde{\phi}_{nl}) + \tilde{\phi}_{nl} \frac{\partial h_{\tilde{l}}(x)}{\partial x} \Big|_{\tilde{\phi}_{nl}} \right] + \left( \frac{n_s}{n_o} \right)^2 h_{\tilde{l}}(\tilde{\phi}_{nl}) \left[ j_{\tilde{l}}(\phi_{nl}) + \phi_{nl} \frac{\partial j_{\tilde{l}}(x)}{\partial x} \Big|_{\phi_{nl}} \right] = 0 \tag{4}$$

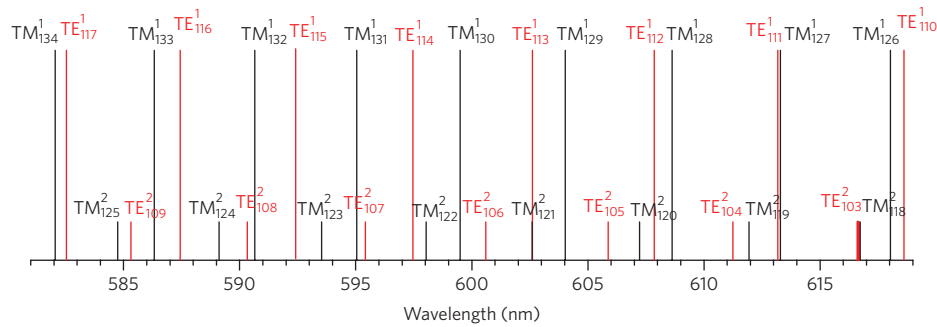
Equation 3 determines the TE mode and equation 4 the TM mode,  $\phi_{nl} = \omega_{nl} n_o a / c$ ,  $\tilde{\phi}_{nl} = \omega_{nl} n_s a / c$ , and  $a$  is radius of the sphere. Interestingly, the characteristic equation for the TE mode in the radial anisotropic sphere is equivalent to the TE mode in an isotropic sphere with the ordinary refractive index, whereas the TM mode couples to both ordinary and extraordinary refractive indices. Note that by making  $n_o = n_e$ , equations 3 and 4 are equivalent to the characteristic equations of an isotropic spherical resonator<sup>20</sup>. Equations 3 and 4 are solved numerically with standard numerical computer packages (for example, Mathematica 7.0).

Figure 3 shows resonant frequencies (wavelengths) of  $n = 1, 2$  TE and TM modes in the experimentally accessible spectral range.

It is interesting that the spectra shows beating of the TE and TM modes, which is caused by the decoupling of the phases in the TE and TM electromagnetic waves and is a direct consequence of TE and TM polarizations experiencing either an ordinary or extraordinary refractive index. For given material parameters ( $n_e = 1.74$ ,  $n_o = 1.52$ ,  $n_s = 1.43$ ) and droplet size  $2a = 15 \mu\text{m}$ , we find a beat frequency (wavelength) of  $\sim 30\text{--}40 \text{ nm}$  in the presented frequency range. The  $n = 1$  and  $n = 2$  modes of single polarization are roughly equidistant in the spectra (spectral distance of two sequential  $n = 1$  and  $n = 2$  mode changes for  $\sim 0.3 \text{ nm}$  over  $\sim 60 \text{ nm}$  spectral range) and can therefore qualitatively be thought as of doublets. This is in agreement with our experimental spectra for larger droplets, presented in Fig. 2b.

### Tuning of WGMs by external electrical field

As the nematic liquid crystals are well known for their very large optical response to external fields, we have applied an external a.c. electric field of frequency 50 kHz to the NLC microresonator, as shown in the schematic drawing in Fig. 4. Figure 4a,b present microphotographs of a 9.3 μm microdroplet, as observed between crossed polarizers at an applied field of  $1.9 V_{\text{RMS}} \mu\text{m}^{-1}$  and  $2.6 V_{\text{RMS}} \mu\text{m}^{-1}$ , respectively. Comparison to the polarized image of the microresonator at zero voltage, shown in Fig. 1b, reveals that large differences in the internal structure of the NLC inside the microresonator have been induced at already moderate fields. The evolution of the radial nematic structure in a spherical microdroplet with increasing electric field has been studied before<sup>18</sup>. Owing to the conservation of topological charge<sup>19</sup>, the radial hedgehog defect, at zero field located in the centre of the droplet, cannot be annihilated, but can be transformed into other defect structures. As a result, the internal structure of the NLC in the microresonator evolves with increasing field, as illustrated in Fig. 4c,d. At moderate fields, the molecules in the interior of the resonator tend to align more and more into the field direction as shown in Fig. 4c, whereas their orientation at the surface is less perturbed. The radial hedgehog point defect is still located at the centre of the droplet, but is now accompanied with a disk-like region of strong distortion, lying in the plane perpendicular to the field. At very high fields, this disk breaks up at a certain threshold voltage and the NLC in the interior of the resonator is nearly perfectly aligned into the field direction. The radial point hedgehog defect opens into a  $+1/2$  defect ring, which is expelled to the surface of the microresonator, and is similar (but of opposite winding number) to the Saturn ring<sup>22</sup>, encircling the resonator at the NLC–PDMS interface.



**Figure 3 | Resonant frequencies (wavelengths) in a dielectrically anisotropic sphere.**  $TE_l^m$  modes are drawn in red, and  $TM_l^m$  modes in black. Observe the characteristic beating of TE and TM modes due to birefringence.

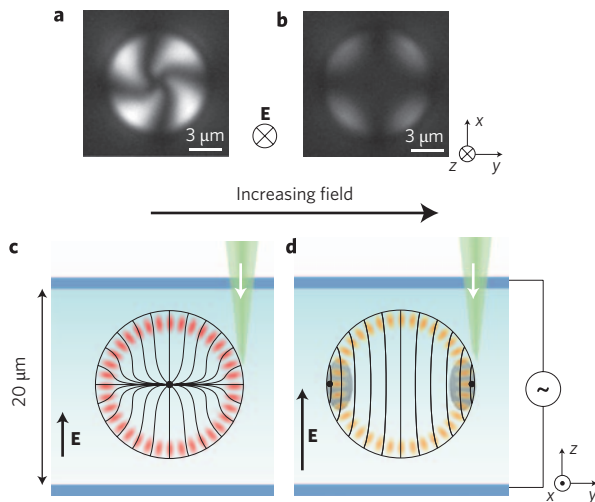


**Figure 4 | Liquid-crystal microresonator in an external electric field.** **a**, Crossed-polarizer micrograph of a  $9.3\ \mu\text{m}$  droplet of E12 in PDMS at  $1.9\ V_{\text{RMS}}\ \mu\text{m}^{-1}$ . **b**, The same droplet at  $2.6\ V_{\text{RMS}}\ \mu\text{m}^{-1}$ . **c, d**, Schematic drawings of the alignment of NLC molecules at different levels of the external electric field.

The electric-field-induced transformation of the internal structure of the NLC, filling the microresonator, should have an important impact on the resonant frequencies of the WGMs. A close look at the orientational distribution of the long axis of the molecules, which is the direction of largest dielectric susceptibility, reveals that the dielectric constant for TM WGM mode is strongly reduced in the region where circulating light of the WGM mode crosses the defect ring (shaded regions in Fig. 4d). This means an effective decrease of the optical path length of the TM WGM, and the WGM resonances should shift towards shorter wavelengths with increasing electric field.

The expected decrease of the wavelength of TM WGM resonances in radial NLC microresonators is indeed observed in the experiments, and is presented in Fig. 5a. At very small fields, there is little influence of the field. Between  $0.5\ V_{\text{RMS}}\ \mu\text{m}^{-1}$  and the voltage where the transition to the  $+1/2$  defect ring occurs, the wavelength-shift decreases nearly linearly with increasing electric field up to  $\sim 3\ V_{\text{RMS}}\ \mu\text{m}^{-1}$ . The shift has no hysteresis and is completely reversible. The switching speed between two wavelengths is limited by the response time of the NLC to the field and is of the order of ten milliseconds. The electric-field-induced WGM shift depends on the diameter of the NLC microresonator, but is as high as  $20\ \text{nm}$  at  $2.6\ V_{\text{RMS}}\ \mu\text{m}^{-1}$  in  $17\ \mu\text{m}$  diameter

radial E12 microresonators, as shown in Fig. 5b. This value is one to two orders of magnitude larger than already published values for electrical tuning. More importantly the spectral shift exceeds the free spectral range, meaning that the resonator frequencies can be shifted to any value. Comparing the tuning range with other techniques, Maune *et al.*<sup>5</sup> report a  $0.22\ \text{nm}$  shift of the WGM resonances in silicon-on-insulator ring resonators by applying  $20\ \text{V}$  across an  $\sim 10\ \mu\text{m}$  electrode gap, where the NLC was used as a tunable cladding layer on top of the ring resonator. Piegdon *et al.*<sup>6</sup> have used 5CB liquid crystal as a cladding layer over  $3\ \mu\text{m}$  GaAs microdisks with InAs quantum dots and found irreversible electric tuning of  $6\ \text{nm}$  at a saturation voltage of  $30\ \text{V}$ . Wang *et al.*<sup>7</sup> report WGM shifts of  $0.4\ \text{nm}$  by applying  $300\ \text{V}$  across an  $\sim 200\ \mu\text{m}$  gap in lithium niobate microring resonators. Kiraz *et al.*<sup>8</sup> report the tuning of WGMs of  $4.7\ \text{nm}$  at  $400\ \text{V}$  in liquid microdroplets standing on a superhydrophobic surface using electro-wetting. We should note that in our experiments, we have not reached the saturation regime at the maximum applied field of  $2.6\ V_{\text{RMS}}\ \mu\text{m}^{-1}$ . For a given droplet, we can however estimate the maximum possible WGM wavelength shift by calculating the decrease of the optical path length between the initial radial configuration and the asymptotic configuration at very high fields. In this asymptotic regime, all molecules are perfectly aligned into the field direction and the optical path length is calculated by integrating the effective index of refraction  $n = (n_o n_e) / \sqrt{n_o^2 \sin^2(\phi) + n_e^2 \cos^2(\phi)}$  around the circumference of the droplet, where simultaneous rotation of the molecular axis by an angle  $\phi$  with respect to the fixed reference frame is considered. For E12, the maximum range of tunability is  $6.7\%$  or  $41\ \text{nm}$  at  $600\ \text{nm}$ .

In addition to the linear increase of WGM frequencies with increasing electric field, we also observe well defined peaks in the intensity of the emitted light at discrete values of the field, shown in Fig. 6a. These intensity peaks are observed when a frequency of a WGM matches the frequency of the incoming  $514\ \text{nm}$  laser light, as described in ref. 23 and schematically presented in Fig. 6b. In this case the resonant coupling between the incoming  $514.5\ \text{nm}$  laser light and the particular WGM mode in resonant condition, increases the amount of light entering the resonator. As the amount of pumping light is strongly increased, this gives rise to the fluorescence intensity of all of the WGM modes and the emitted intensity increases strongly. The LC microdroplet resonator therefore acts as a light valve, redirecting the incoming laser light, and is in fact a conceptual step towards the realization of the microcavity add-drop filter<sup>2</sup>. Whereas energy transfer in add-drop filters is realized in the near field—that is, by tunnelling of light across the gap, separating the ring resonator and the waveguide—we have here a ‘far-field’ realization of the add-drop filter, where the resonant transfer of energy is of the same nature and

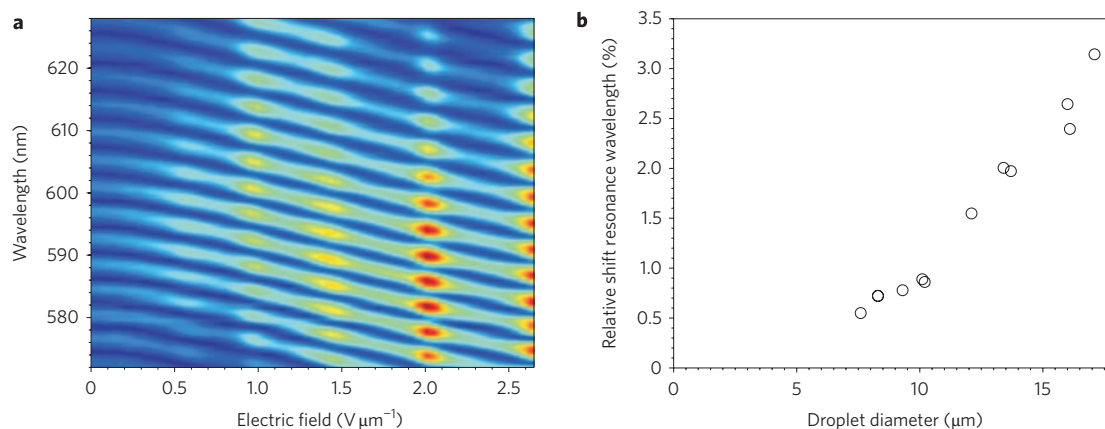


**Figure 5 | Electric-field-induced shift of TM WGM resonances.** **a**, Wavelength shift in a 16-μm-diameter microresonator, filled with E12 nematic liquid-crystal and SPP-106 fluorescent dye. The colour scale indicates the intensity of detected light. Note the enhancement of the resonances at discrete wavelengths. **b**, Range of tunability of E12 microresonators as a function of droplet diameter, determined at  $2.6 V_{\text{RMS}} \mu\text{m}^{-1}$ .

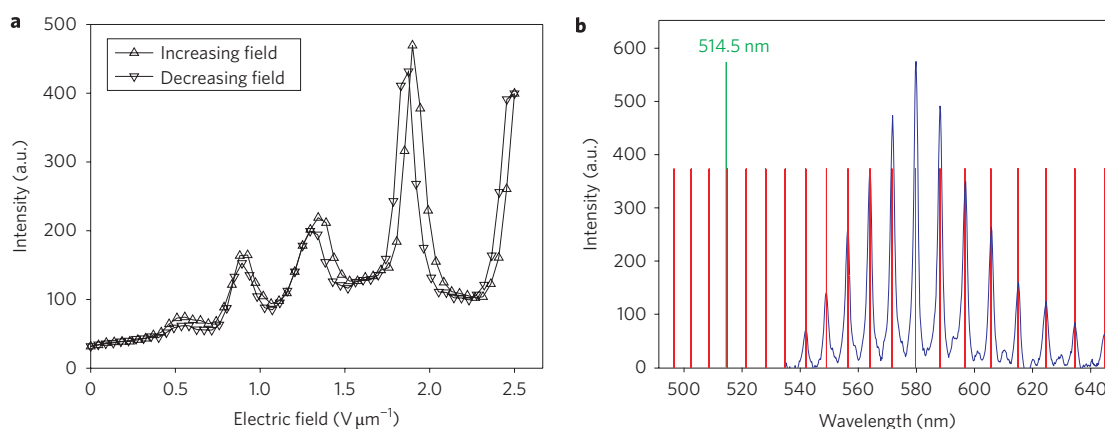


**Figure 6 | Electric tuning of the resonant transfer of external light to the liquid-crystal microcavity.** **a**, Integral intensity, radiated from the LC microcavity, as a function of the applied electric field. Note the intensity increase at discrete values of the electric field. **b**, Principle of resonant transfer of light through tunable LC microcavity. Red vertical lines represent WGM resonances of the microcavity. When the external electric field is applied, this set of resonances shifts as a whole towards shorter wavelengths. When the Ar<sup>+</sup> line (green vertical line) matches a particular WGM, external light is resonantly coupled into the resonator, and the fluorescent emission of all WGM modes is strongly enhanced.

appears when the cavity resonant frequency matches that of the incoming light field.

## Conclusions

In conclusion, we have demonstrated for the first time the use of LC droplets as tunable optical microresonators with high  $Q$ -factors. The electric-field tunability of WGM resonances is two orders of magnitude larger than has previously been known and  $Q$ -factors up to  $\sim 12,000$  have been observed. Linear and reversible electrical tuning is obtained, exceeding the free spectral range of the resonator. Tuning ranges up to 40 nm at reasonable voltages could be obtained with proper selection of LC materials. A theoretical analysis of optical eigenmodes in a birefringent radial microresonator has been performed, which is in qualitative agreement with experiments. We have also demonstrated resonant transfer of light, which can be controlled with an external electric field. The advantage of LC microresonators is the simplicity of their self-formation, their surprisingly high  $Q$ -factor and their large response to external stimuli including low electric fields. In view of very low losses, observed with radial nematic LC microcavities, a new concept of light manipulation using soft matter has been demonstrated, which could be extended to voltage-tunable optical microdevices,

surface-sensitive sensors, tunable microcavity lasers and soft matter photonic circuits.

## Methods

A solution of fluorescent dye SPP-106 (rhodamine B tetradecyl ester chloride) in E12 was prepared as a resonator medium. E12 exhibits a nematic phase in the temperature range of  $-10$  °C to  $59$  °C. The refractive indices at room temperature are  $n_o = 1.52$  and  $n_e = 1.74$  at 590 nm. SPP-106 has advantages over plain rhodamine B, as the non-polar tail of the dye ensures better solubility in the liquid crystal and prevents the diffusion of the dye into the surrounding PDMS polymer.

PDMS polymer (Sylgard 184, Dow Corning) was then prepared by mixing a 10:1 mass ratio of liquid silicon base and a curing agent. The LC was introduced to PDMS and mechanically stirred forming small polydispersed droplets of sizes in the range of  $1 \mu\text{m}$ – $20 \mu\text{m}$ . The mixture was enclosed into thin glass cells. These were made from glass slides, covered with a thin indium-tin-oxide (ITO) layer, serving as an electrode. Two glass slides were sandwiched into a cell, where the cell-gap was controlled by polymer spacer of thickness  $20 \mu\text{m}$  and the ITO electrodes were in the interior. Prior to measurements the samples were left for 48 hours at room temperature so that the PDMS polymer completely crosslinked.

To excite the WGM inside the LC droplets, an Ar<sup>+</sup> (514 nm) laser tweezers setup was used. The laser light was focused by a  $60\times$  water immersion objective to a submicrometre spot near the edge of the droplet. The fluorescent light was collected through the same objective and sent through an optical fibre to the spectrophotometer. An Ocean Optics USB4000 spectrophotometer with spectral resolution of 1.5 nm and an Ocean Optics Maya 2000 Pro with spectral resolution of 0.03 nm were used. During the spectra collection, an external AC voltage of

0–2.6  $V_{\text{RMS}} \mu\text{m}^{-1}$  and frequency of 50 kHz was applied to the PDMS layer containing the droplets. High-resolution linewidth measurements were performed on a Horiba Jobin Yvone LabRAM HR800 Raman spectrophotometer equipped with a multi-channel, air cooled CCD detector, coupled to an Olympus BXFM optical microscope. The resolution of the spectrophotometer was 0.019 nm per detector pixel. The acquisition time was 1 s.

Received 23 February 2009; accepted 25 August 2009;  
published online 27 September 2009

## References

- Ashkin, A. & Dziedzic, J. M. Observation of resonances in the radiation pressure on dielectric spheres. *Phys. Rev. Lett.* **38**, 1351–1354 (1977).
- Vahala, K. J. Optical microcavities. *Nature* **424**, 839–846 (2003).
- Kiraz, A., Kurt, A. & Dundar, M. A. Simple largely tunable optical microcavity. *Appl. Phys. Lett.* **89**, 081118 (2006).
- Saito, M., Shimatani, H. & Naruhashi, H. Tunable whispering gallery mode emission from a microdroplet in elastomer. *Opt. Express* **16**, 11915–11919 (2008).
- Maune, B., Lawson, R., Gunn, C., Scherer, A. & Dalton, L. Electrically tunable ring resonators incorporating nematic liquid crystals as cladding layers. *Appl. Phys. Lett.* **83**, 4689–4691 (2003).
- Piegdon, K. A., Matthias, H., Meier, C. & Kitzerow, H.-S. Tunable optical properties of photonic crystals and semiconductor microdisks using liquid crystals. *Proc. SPIE Int. Soc. Opt. Eng.* **6911**, 6911OJ (2008).
- Wang, T.-J., Chu, C.-H. & Lin, C.-Y. Electro-optically tunable microring resonators on lithium niobate. *Opt. Lett.* **32**, 2777–2779 (2007).
- Kiraz, A., Karadag, Y. & Coskun, A. F. Spectral tuning of liquid microdroplets standing on superhydrophobic surface using electrowetting. *Appl. Phys. Lett.* **92**, 191104 (2008).
- de Gennes, P. G. & Prost, J. *The Physics of Liquid Crystals* 2nd ed. (Oxford Science, 1993).
- Song, M. H. *et al.* Electrotunable non-reciprocal laser emission from a liquid-crystal photonic device. *Adv. Funct. Mater.* **16**, 1793–1798 (2006).
- Hands, P. J. W. *et al.* Two-dimensional liquid crystal laser array. *Opt. Lett.* **33**, 515–517 (2008).
- Munoz, A. F., Palfy-Muhoray, P. & Taheri, N. Ultraviolet lasing in cholesteric liquid crystals. *Opt. Lett.* **26**, 804–806 (2001).
- Moreira, M. F. *et al.* Cholesteric liquid-crystal laser as an optic fiber-based temperature sensor. *Appl. Phys. Lett.* **85**, 2691–2693 (2004).
- Cao, W., Munoz, A., Palfy-Muhoray, P. & Taheri, B. Lasing in a three-dimensional photonic crystal of the liquid crystal blue phase II. *Nature Mater.* **1**, 111–113 (2002).
- Morris, S. M., Ford, A. D., Pivnenko, M. N. & Coles, H. J. Enhanced emission from liquid crystal lasers. *J. Appl. Phys.* **97**, 023103 (2005).
- Humar, M. *et al.* Electrically tunable diffraction of light from 2D nematic colloidal crystals. *Eur. Phys. J. E* **27**, 73–79 (2008).
- Doane, J. W., Vaz, N. A., Wu, B.-G. & Žumer, S. Field controlled light scattering from nematic microdroplets. *Appl. Phys. Lett.* **48**, 269–271 (1986).
- Bodnar, V. G., Lavrentovich, O. D. & Pergamenschchik, V. M. Threshold of structural hedgehog-ring transition in drops of a nematic in an alternating electric field. *Sov. Phys. JETP* **74**, 60–67 (1992).
- Stark, H. Physics of colloidal dispersions in nematic liquid crystals. *Phys. Rep.* **351**, 387–474 (2001).
- Novotny, L. & Hecht, B. *Principles of Nano-Optics* (Cambridge University Press, 2006).
- Cohoon, D. K. An exact solution of Mie type for scattering by a multilayer anisotropic sphere. *J. Electromagnet. Wave.* **3**, 421–448 (1989).
- Gu, Y., Abbott, N. L. Observation of Saturn-ring defects around solid microspheres in nematic liquid crystals. *Phys. Rev. Lett.* **85**, 4719–4722 (2000).
- Eversole, J. D., Lin, H.-B. & Campillo, A. J. Input/output resonance correlation in laser-induced emission from microdroplets. *J. Opt. Soc. Am. B* **12**, 287–296 (1995).

## Acknowledgements

The authors would like to thank P. Ropret, S. Žumer, M. Škarabot, S. Pečar, J. Pirš and J. Štrancar for their help and suggestions. This work was supported by the Slovenian Research Agency under the contracts P1-0099 and J1-9728.

## Author contributions

M.H. performed all experiments and analysed the results. M.R. has carried out the theoretical calculations. S.P. synthesized the SPP-106 dye. I.M. initiated the work on WGM resonances in LC droplets, organized and supervised the experiments. M.H., M.R. and I.M. wrote the manuscript.

## Additional information

Supplementary information accompanies this paper at [www.nature.com/naturephotonics](http://www.nature.com/naturephotonics). Reprints and permission information is available online at <http://npg.nature.com/reprintsandpermissions/>. Correspondence and requests for materials should be addressed to I.M.